Supplemental Figures

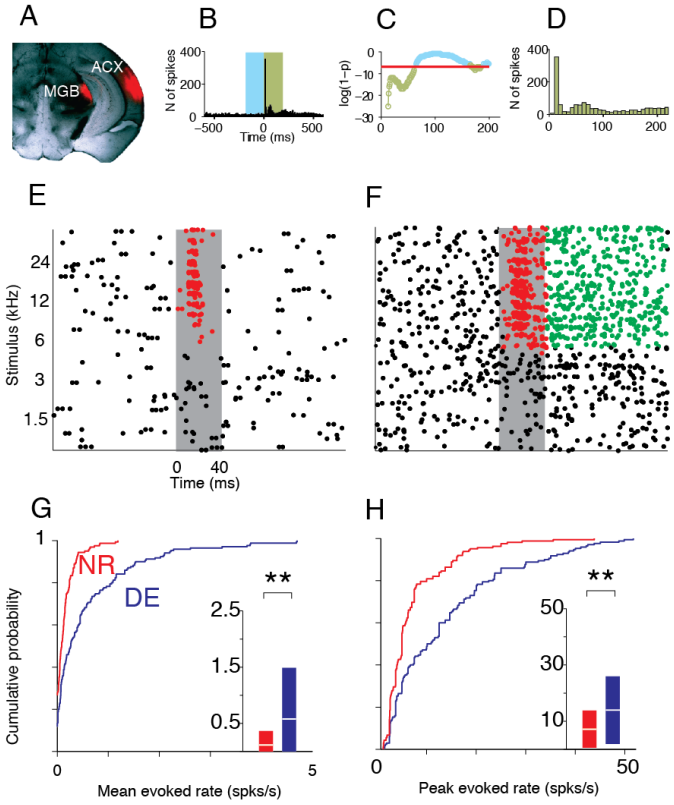

Fig. S1 (related to Fig. 1). Location of recording and isolation of responses by the binless algorithm. (**A**) Recording site in A1 is confirmed by retrograde labeling of MGB with DiI placed at the recording location. (**B**) Representative peri-stimulus time histogram (PSTH) with a response window (green, 200 ms post-stimulus) and spontaneous window (blue, 200 ms pre-stimulus). (**C**) *log*(1-probability) of responses as function of time obtained by the binless algorithm at a temporal resolution of 10 ms, with threshold of significance indicated by red line. Activity below this threshold was considered significant. (**D**) PSTH derived from (**B**), showing activity only following the stimulus. (**E, F**) Raster-plot showing driven activity with both brief (red**, E**) and prolonged responses seen **(**green, **F).** Grey box indicates stimulus duration. (**G, H**) Comparisons of initial response characteristics within the early response window. Cumulative distribution functions showing comparisons of mean (**G**) and peak (**H**) evoked rates within an

early response window (0-75 ms following stimulus onset). Both mean and peak rates show considerable increases (NR in red, DE in blue), and the change in mean evoked rate is in sharp contrast to those seen globally (**B**). Asterisks indicate levels of significance by one way analysis of variance (ANOVA). Details of statistical comparisons are provided in text.

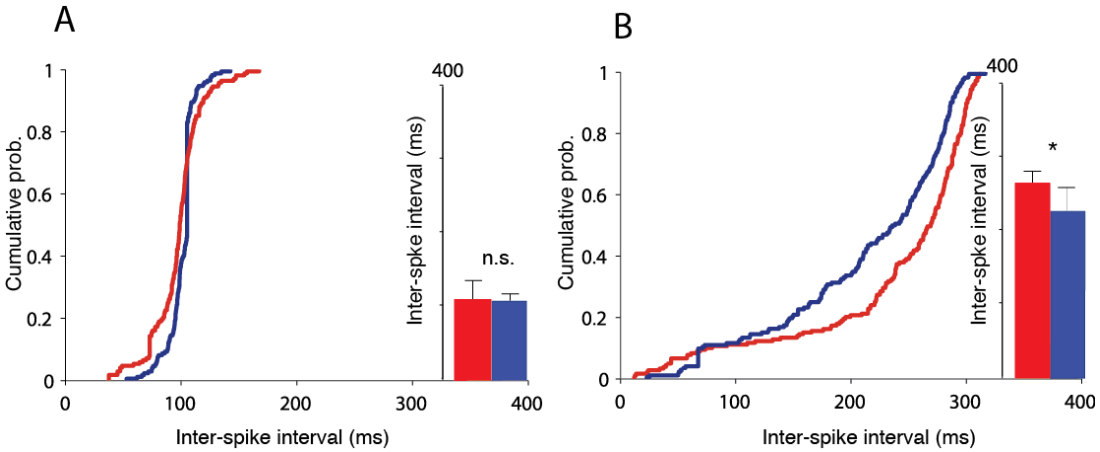

Fig. S2 (related to Fig. S1). Comparison of inter-spike intervals (ISIs). (A) and (B) show cumulative probability distributions of ISIs as compared between NR (red) and DE (blue) for spontaneous activity (-200 to 0 ms) and activity following onset of stimulus (0-600 ms). While the differences were not significant for spontaneous activity, DE units had significantly reduced ISI (ANOVA, $P < 0.05$) for the responses recorded during the 600 ms following onset of stimulus. The first spike latency (**Fig. 1C**) is significantly shorter than spontaneous ISI (A, ANOVA, $P < 0.001$).

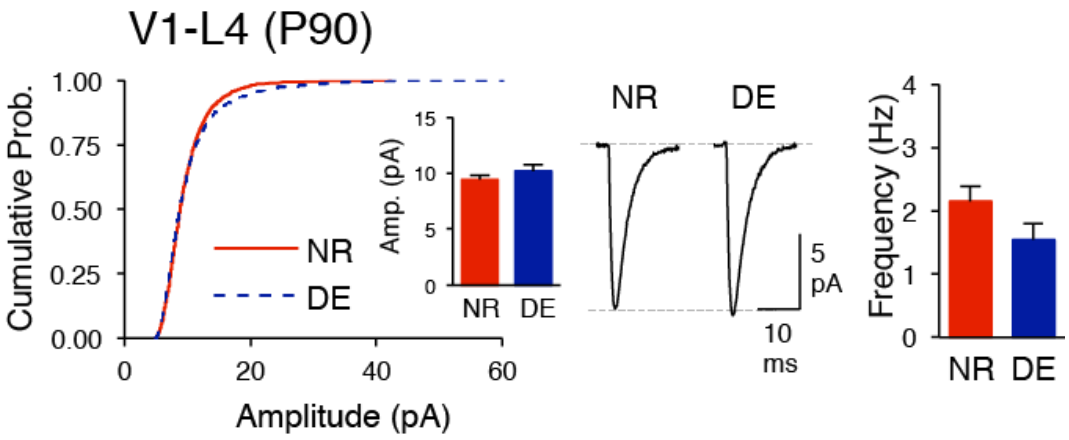

Fig. S3 (related to Fig. 3). Absence of a regulation of mEPSCs in V1 L4 in adults (P90). Left: Cumulative probability of mEPSC amplitudes. Inset: Average mEPSC amplitude. Middle: Average mEPSC traces. Right: Average mEPSC frequency.

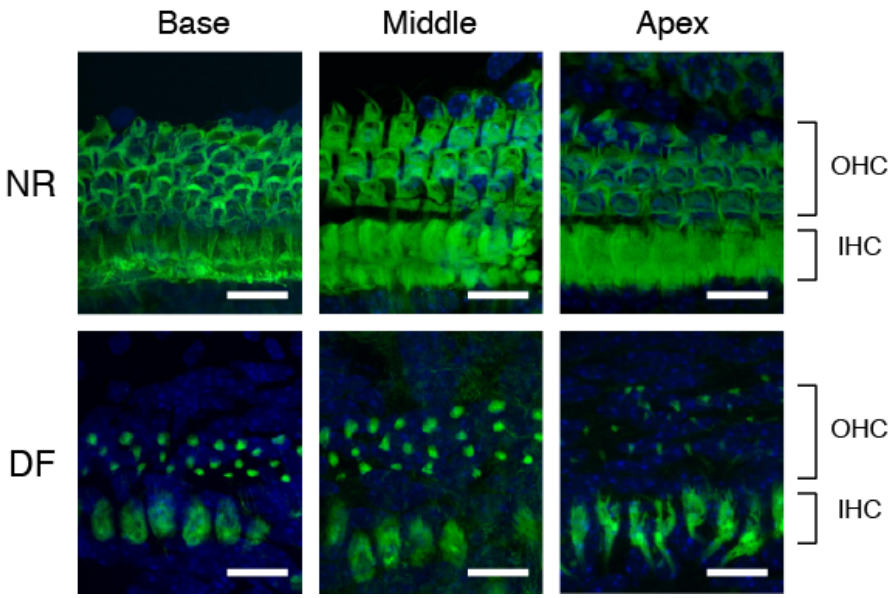

Fig. S4 (related to Fig. 5). Confirmation of cochlear damage by phalloidin staining of hair cells. Alexa488-conjugated phalloidin staining (green) of cochlear hair cells from a normal-reared (NR) mouse (top panels) and a deaf (DF) mouse (bottom panels). Sections were counterstained with DAPI (blue). Sections were taken from the basal, middle, and apical portions of the cochlea. Note abnormal degenerated hair cells in the DF samples. OHC: outer hair cells. IHC: inner hair cells. Scale Bars: 15 μm.

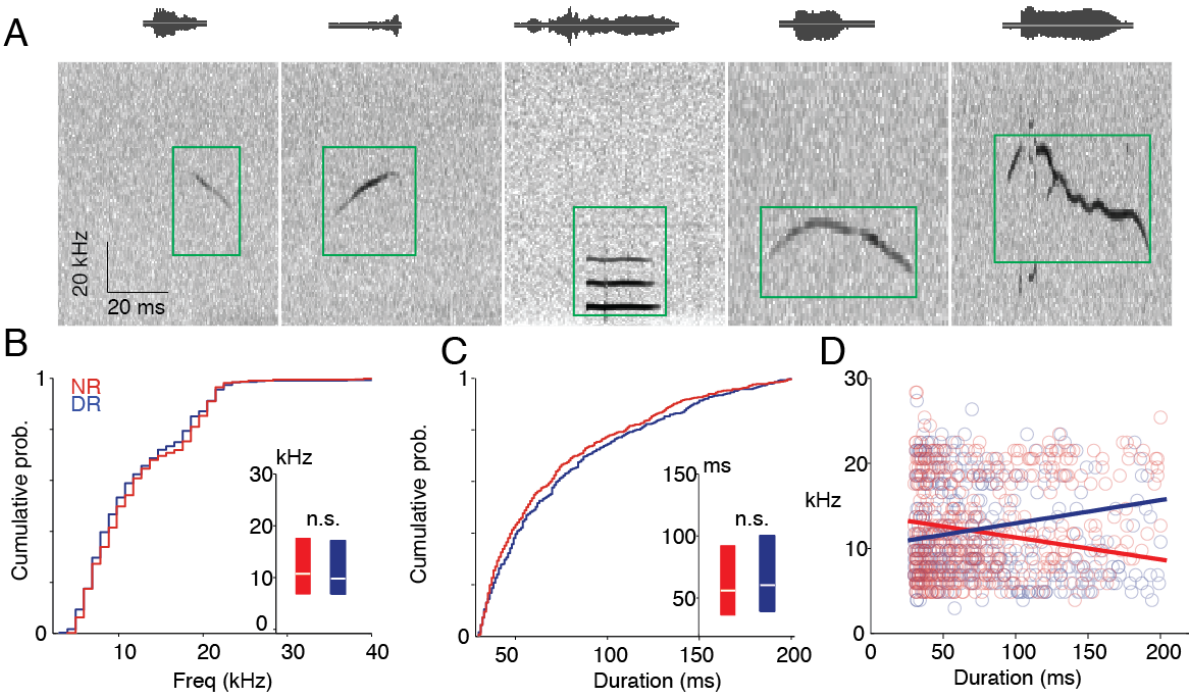

Fig. S5 (related to Fig. 4,5). Comparisons of vocalizations under each rearing condition. (**A**) Spectrograms of detected vocalizations. Green boxes indicate analyzed time window. 5 main calls were distinguished: upgoing, downgoing, chevron, flat/harmonic and unstructured. (**B, C**) Peak frequencies (**B**) and durations (**C**) of calls were measured. There were no significant differences either peak frequencies ($F_{1,969} = 2.36$, $P = 0.13$, ANOVA) or durations ($F_{1,969} = 0.53$, $P = 0.47$, ANOVA) of these calls. (**D**)The slopes of linear functions plotted for frequency vs. duration also were not significantly different from each other ($F_{1,967} = 0.58$, $P = 0.45$).

Supplemental Tables

Area	Conditions	Paradigm	Amplitude (pA)	Frequency (Hz)	Rise Time (ms)	Decay τ (ms)	Series R (MΩ)	Input R (MΩ)	RMS Noise
A1	PreLED	NR	10.0 ± 0.46	2.8 ± 0.25	1.9 ± 0.06	2.5 ± 0.28	19.1 ± 1.2	238 ± 41	1.4 ± 0.06
		7d-DE	11.6 ± 1.27	2.9 ± 0.25	1.9 ± 0.04	2.6 ± 0.25	22.4 ± 0.8	175 ± 20	1.4 ± 0.07
		7d-LE	10.1 ± 0.45	4.0 ± 0.42	1.7 ± 0.06	2.9 ± 0.20	19.4 ± 1.0	182 ± 18	1.6 ± 0.05
	PostLED	NR	10.2 ± 0.40	3.5 ± 0.29	1.8 ± 0.06	2.2 ± 0.14	19.1 ± 1.2	238 ± 41	1.4 ± 0.05
		7d-DE	14.6 ± 1.3*	5.0 ± 0.31	1.8 ± 0.05	2.7 ± 0.20	22.4 ± 0.8	175 ± 20	1.4 ± 0.07
		7d-LE	10.9 ± 0.56	6.3 ± 0.76	1.7 ± 0.04	2.8 ± 0.22	19.4 ± 1.0	182 ± 18	1.6 ± 0.05
	Calculated TC-mEPSCs	NR (n = 14)	12.8 ± 1.3	–	–	–	–	–	–
		7d-DE (n = 12)	25.7 ± 4.4*	–	–	–	–	–	–
		7d-LE (n = 14)	13.7 ± 1.4	–	–	–	–	–	–
V1	PreLED	NR	11.4 ± 0.52	3.6 ± 0.37	1.7 ± 0.06	3.1 ± 0.20	18.9 ± 1.4	283 ± 52	1.6 ± 0.07
		7d-DE	10.5 ± 0.77	3.5 ± 0.23	1.8 ± 0.04	3.3 ± 0.17	19.0 ± 1.4	175 ± 24	1.4 ± 0.07
	PostLED	NR	11.6 ± 0.46	5.0 ± 0.44	1.7 ± 0.07	3.2 ± 0.19	18.9 ± 1.4	283 ± 52	1.6 ± 0.07
		7d-DE	11.7 ± 0.97	5.6 ± 0.43	1.8 ± 0.06	3.1 ± 0.18	19.0 ± 1.4	175 ± 24	1.4 ± 0.07
	Calculated TC-mEPSCs	NR (n = 11)	11.3 ± 0.93	–	–	–	–	–	–
		7d-DE (n = 12)	13.4 ± 1.43	–	–	–	–	–	–

Table S1. Comparison of thalamocortical Sr^{2+}-mEPSC parameters with dark exposure. *Denotes statistically significant difference from corresponding NR; $P < 0.05$ for one-factor ANOVA followed by Fisher's PLSD post-hoc test.

Area	Age	Paradigm	n	Amplitude (pA)	Frequency (Hz)	Rise Time (ms)	Decay τ (ms)	Series R (MΩ)	Input R (MΩ)	RMS Noise
A1	P28	NR	15	10.9 ± 0.67	3.0 ± 0.44	1.8 ± 0.05	3.1 ± 0.12	18.5 ± 1.3	161 ± 10	1.7 ± 0.04
		7d-DE	19	13.4 ± 0.70*	3.7 ± 0.34	1.7 ± 0.03	3.1 ± 0.1	19.2 ± 2	224 ± 21	1.7 ± 0.04
		7d-LE	15	10.7 ± 0.50	2.5 ± 0.25	1.8 ± 0.03	3.1 ± 0.1	20.0 ± 0.7	193 ± 20	1.6 ± 0.05
	P90	NR	17	10.7 ± 0.41	2.8 ± 0.24	1.8 ± 0.03	3.1 ± 0.1	21.1 ± 0.9	174 ± 13	1.7 ± 0.03
		7d-DE	13	12.9 ± 0.75*	1.5 ± 0.17	1.9 ± 0.04	3.2 ± 0.1	21.7 ± 0.6	200 ± 19	1.6 ± 0.04
		7d-LE	14	10.8 ± 0.40	2.4 ± 0.26	1.8 ± 0.03	3.1 ± 0.1	21.6 ± 0.7	234 ± 27	1.6 ± 0.04
	CBA P90	NR	12	10.2 ± 0.49	5.0 ± 0.35	1.6 ± 0.05	2.8 ± 0.1	18.6 ± 0.8	160 ± 18	1.7 ± 0.06
		7d-DE	16	11.7 ± 0.32*	5.1 ± 0.41	1.6 ± 0.02	2.8 ± 0.1	22.3 ± 0.8	197 ± 21	1.7 ± 0.4
V1	P90	NR	15	9.4 ± 0.43	2.1 ± 0.24	1.8 ± 0.04	3.3 ± 0.1	19.0 ± 0.9	208 ± 19	1.6 ± 0.05
		7d-DE	13	10.2 ± 0.56	1.6 ± 0.24	1.8 ± 0.03	3.4 ± 0.1	19.2 ± 1	184 ± 20	1.6 ± 0.04

Table S2. Comparison of L4 mEPSC parameters. *Denotes statistically significant difference from corresponding NR; $P < 0.05$ for one-factor ANOVA followed by Fisher's PLSD post-hoc test.

Area	Conditions	Paradigm	Amplitude (pA)	Frequency (Hz)	Rise Time (ms)	Decay τ (ms)	Series R (MΩ)	Input R (MΩ)	RMS Noise
A1	PreLED	NR	9.3 ± 0.9	3.1 ± 0.3	1.6 ± 0.1	3.3 ± 0.3	20.7 ± 1.1	215 ± 29	1.6 ± 0.1
		7d-DF	12.0 ± 0.7*	4.5 ± 0.4*	1.8 ± 0.1	3.1 ± 0.1	21.3 ± 1.1	197 ± 18	1.6 ± 0.1
		7d-DD	12.4 ± 0.8*	5.1 ± 0.5*	1.8 ± 0.04	3.2 ± 0.2	21.4 ± 1.0	186 ± 15	1.6 ± 0.1
	PostLED	NR	12.0 ± 0.9	9.3 ± 1.4	1.7 ± 0.1	2.9 ± 0.2	20.7 ± 1.1	215 ± 29	1.6 ± 0.1
		7d-DF	12.6 ± 0.5	7.8 ± 0.7	1.8 ± 0.04	3.3 ± 0.2	21.3 ± 1.1	197 ± 18	1.6 ± 0.1
		7d-DD	13.0 ± 1.2	8.8 ± 0.7	1.8 ± 0.04	3.1 ± 0.2	21.4 ± 1.0	186 ± 15	1.6 ± 0.1
	Calculated TC-mEPSCs	NR (n = 9)	13.5 ± 0.9	–	–	–	–	–	–
		7d-DF (n = 12)	13.5 ± 1.8	–	–	–	–	–	–
		7d-DD (n = 14)	15.4 ± 1.9	–	–	–	–	–	–
V1	PreLED	NR	10.2 ± 0.7	4.0 ± 0.5	1.6 ± 0.1	3.0 ± 0.3	22.4 ± 0.6	206 ± 27	1.5 ± 0.1
		7d-DF	9.8 ± 0.4	4.0 ± 0.5	1.7 ± 0.1	3.0 ± 0.2	21.7 ± 1.2	206 ± 30	1.5 ± 0.1
	PostLED	NR	11.8 ± 0.9	7.9 ± 1.3	1.7 ± 0.1	2.9 ± 0.2	22.4 ± 0.6	206 ± 27	1.5 ± 0.1
		7d-DF	14.4 ± 1.1	8.8 ± 1.1	1.8 ± 0.1	3.0 ± 0.1	21.7 ± 1.2	206 ± 30	1.5 ± 0.1
	Calculated TC-mEPSCs	NR (n = 11)	12.7 ± 1.2	–	–	–	–	–	–
		7d-DF (n = 10)	18.8 ± 1.6*	–	–	–	–	–	–

Table S3. Comparison thalamocortical Sr^{2+}-mEPSC parameters with deafening. *Denotes statistically significant difference from corresponding NR; $P < 0.05$ for one-factor ANOVA followed by Fisher's PLSD post-hoc test for A1, student's t-test for V1.

Experimental Procedures

Animals

Male and female C57BL/6J mice (Jackson Laboratories) were raised in 12-hr light/ 12-hr dark conditions. At P21 or P90 mice (2-3 mice from established litters and single gender per cage) were dark exposed (DE) for 7 days. Age-matched controls remained in normal light conditions (NR). We measured ambient sound levels with a calibrated sound meter and vocalizations with an ultrasonic microphone (Avisoft UltraSoundGate 116H with Avisoft CM16; sampling rate of 250 kHz and for approximately 20 hours in each condition). Ambient sound levels (40-43 dB) were similar under both rearing conditions. Vocalizations were manually tagged in spectrograms using criteria previously established (Grimsley et al., 2011). Peak frequencies and durations were measured after 5 main types of calls were isolated in recordings (**Fig. S6A**; upgoing, downgoing, chevron, flat/harmonic and unstructured). A total of 971 calls were analyzed (428 in DE and 543 in NR condition). There were no significant differences either in durations of these calls or peak frequencies (**Fig. S6B-C**, duration; $F_{1,969} = 2.36$, $P = 0.13$ and frequency; $F_{1,969} = 0.53$, $P = 0.47$, ANOVA). The slopes of linear functions plotted for frequency vs. duration also were not significantly different (Fig. S6D, $F_{1,967} = 0.58$, $P = 0.45$). DE animals were cared for using infrared vision goggles with dim infrared light. Some mice were returned to normal light conditions for 7 days to study the effect of light re-exposure (LE). CBA/CaJ (CBA) mice were obtained from Jackson Laboratories and were DE or NR at P90. All experiments were approved by the Institutional Animal Care and Use Committees (IACUCs) of Johns Hopkins University and University of Maryland and followed the guidelines of the Animal Welfare Act.

Channelrhodopsin-2 (ChR2) Viral Transfection

P21 mice were anesthetized with 1-3% isoflurane mixed with O_2 and transcranially injected bilaterally with 1.5 µl adeno-associated virus containing channelrhodopsin-2 and yellow fluorescence protein as a marker (AAV2/9.hSynapsin.hChR2(H134R)-EYFP.WPRE.hGH, Addgene26973, Penn Vector Core) into MGB (auditory) thalamus at coordinates: Bregma 1.8, Lateral 2.9, Depth 3.25 or dorsal LGN (visual) thalamus at coordinates: Bregma 2.3, Lateral 2.0, Depth 2.42. Mice recovered on a heated surface and were returned to the animal colony, where they remained for 6-8 weeks to produce optimal ChR2 expression before experimental paradigms were initiated.

Deafening

Experimental mice were initially anesthetized with isofluorane vapors (3%), after which a moderate plane of anesthesia was maintained (1.5% flow). Mice were placed in a stereotaxic apparatus (David Kopf Instruments, California) and rotated to their side so one ear at a time faced up. Pinnae were removed and incisions were made to the ventral surface to enhance visualization of ear anatomy. Using a dissection microscope the tympanic membrane was incised using a 30 gauge needle. Ossicles were moved to the side to visualize the round window. 50 µl kanamycin solution (175 mg/ml saline) was infused into the inner ear, and a small piece of gelfoam (Pfizer) soaked in kanamycin solution was placed in the inner ear (Hashimoto et al., 2007). Incisions were sutured (PDS II: Ethicon) closed and animals were allowed to recover on a warm heat pad and returned to their cage after recovery from anesthesia. Animals were kept no more than 3 per cage, and were sacrificed between 6-8 days post procedure. Deafening was confirmed by behavioral absence of acoustic startle with 90 dB sound and histological

observation of hair cell loss using phalloidin staining. One mouse was removed from the experiment due to unsuccessful deafening procedures. To do the staining, whole cochleae were removed from experimental animals and submerged in cold 4% PFA for 2 hours. 0.5 ml of 4% PFA were injected through the round window to ensure complete fixation. Cochleae were washed 3 times in 0.1 M PB and decalcified in 5% EDTA overnight. The samples were then sunk in 30% sucrose overnight and sectioned on a sliding microtome (Microtome HM400, Midwest Lab Equipment, Florida) at 60-µm thickness. Slices were permeabilized in 0.2% Triton in 0.1M PB for 1 hour, followed by staining with Alexa Fluor 488-phalloidin (Invitrogen) at 1:200 dilution for 2 hours. Slices were also counterstained for DAPI at 1:5000 dilution (Invitrogen). Cochlear slices were mounted on glass slides and cover-slipped using ProLong Gold antifade reagent (Life Technologies). Confocal z-stacks were obtained using a Zeiss LSM510 Meta confocal microscope. Destruction of hair cells was verified for all deafened animals, and the presence of intact hair cells was verified for all control animals (**Fig. S4**).

In vivo recordings

Animals were prepared for recordings after induction and maintenance with isoflurane (2%). Paw-pinch reflex was monitored for ensuring an adequate plane of anesthesia. Craniotomy was performed using standard anatomical landmarks and dura was incised to expose A1. A digitally-controlled micromanipulator (Sutter Instrument, CA) was used to insert and record depths of penetration of 16-channel single-shank silicon probes (CM16, Neuronexus, MI) within the middle cortical layers of A1 (**Fig. S1A**), orthogonally to the cortical surface. The distributions of depths were normally distributed and similar for both groups (NR [n=173] mean

= 509.60 µm, s.d. = 234.02; DE [n=175] mean = 519.97 µm, s.d. = 213.04; $F_{1,347} = 0.19$, $P = 0.67$, ANOVA).

Computer-generated stimuli were produced using custom software written in Matlab (Natick, MA) and presented via a calibrated free-field speaker (Tucker Davis Technologies, Alachua, FL). 21 log-spaced pure tones (40 ms, 1-35 kHz) were presented at 10 dB steps from 10-70 dB SPL and repeated 10 times in a randomly interleaved fashion. Recordings were obtained using Cheetah-32 hardware (Neuralynx, MT) and spike sorting was performed offline using *KlustaKwik* (http://neuro.debian.net/pkgs/klustakwik.html) software. Separation into single-units and small multi-unit clusters was carried out by unsupervised clustering with a Gaussian mixture model with unconstrained covariance matrices (Harris et al., 2000). A group of similar waveforms was considered as being generated from a single neuron if it defined a discrete cluster in a 2D/3D space of principal components. Spike sorting yielded roughly equal number of units (NR=175; DE=173) for both groups of animals.

Raw data was exported to Matlab software for further analysis. Significant neuronal responses were first identified by Chase and Young's adaptation (Chase and Young, 2007) of the well-known Victor's binless method (Victor, 2002). This algorithm searches, via a sliding window of chosen temporal precision (1, 10 and 50 ms) for significant neuronal responses within the succeeding inter-stimulus interval for up to 600 ms and compares responses to those seen within the immediate pre-stimulus window for up to 200 ms prior to stimulus onset, treating the latter as a *Poisson* process (e.g., **Fig. S1B, C**). The binless algorithm, adapted for use for computation of first-spike latency statistics (Chase and Young, 2007) used the following method

to distinguish spontaneous from stimulus-driven spikes. In summary, this technique compares the observed response over the pooled PSTH of all responses with the expected response assuming that the spontaneous firing of a neuron follows *Poisson* statistics. Under the *Poisson* assumption, the probability of observing a response of at least n spikes in a window t_n is

$$Pt_n(\geq n) = 1 - \sum_{m=0}^{n-1} \frac{(N\lambda t_n)^m e^{-N\lambda t_n}}{m!} \qquad \textbf{Equation 1}$$

where λ is the spontaneous rate; and the latency to the first spike that is deemed to show significant deviation from the driving rate is computed with a set threshold of 10^{-6} (red horizontal line in **Fig. S1B**). Given the evidence that suggests that spike rates continue to be modulated for a significant period of time following the onset of an auditory stimulus even for brief sounds (Campbell et al., 2010; Walker et al., 2011), we set a window length of 600 ms following the stimulus onset to search for spikes while the 200 ms preceding the stimulus was considered spontaneous neural activity, identifying periods of significant neural responses (**Fig. S1D**). Both brief and prolonged (**Fig. S1E, F**) responses were observed in both groups of animals. Peak and mean evoked rates, spontaneous activity, latency of first spikes (**Fig. 1**) and slopes of rate-level functions (**Fig. 2**) were calculated from this data and statistically analyzed using analysis of variance (ANOVA). Although the mean evoked rates were unchanged between groups (NR= –0.05 spikes/s, s.d. = 0.17; DE= –0.02 spikes/s, s.d.=0.34; $F_{1,332}$=0.65, P =0.42), peak rates improved dramatically (NR=1.58 spikes/s, s.d.=1.60; DE=3.84 spikes/s, s.d.=5.43; $F_{1,332}$=26.06, P <10^{-6}). This was in contrast to activity the first 75 ms (**Fig. S1G, H**) wherein the initial responses were seen. DR cells showed higher mean (**Fig. S1G**) and peak (**Fig. S1H**) evoked spike rates when compared with NR cells within this window.

Spontaneous activity increased (NE = 0.23 spikes/s, s.d. = 0.35; DE = 0.55 spikes/s, s.d. = 0.99; $F_{1,324} = 14.82$, $P = 0.0001$) while the response latency was reduced (NR = 2.74 ms, SD = 1.23; DE = 0.99 ms, SD = 4.81; $F_{1,332} = 4.77$, $P = 0.03$). The slopes of rate-level functions (e.g. **Fig. 2B**) were compared by fitting linear regressions and showed a significant increase with DE (mean zero order slope for NR = 0.19 spikes/s/dB SPL, s.d. = 0.20; DE = 0.46 spikes/s/dB SPL, s.d. = 0.36; $F_{1,296} = 37.56$, $P < 10^{-8}$). Next, tuning characteristics were determined (**Fig. 2B-D**) by analysis of frequency response area (FRA) functions (e.g. **Fig. 1A**). A unit was classified as tuned if the bandwidth (BW) at 10 dB above threshold was < 3 octaves in reference to the CF, and showed a single predominant peak only. These were further analyzed for properties such as threshold, characteristic frequency (CF), quality factors at 10 dB and 40 dB above threshold (Q10, Q40). Of these, threshold was reduced with DE (NR = 39.42 dB SPL, s.d. = 12.4; DE = 35.11 dB SPL, $F_{1,219} = 6.83$, $P = 0.0096$), and Q10 revealed a significant increase in sharpness of tuning (NR = 0.74, s.d. = 0.46; DE = 0.91, s.d. = 0.46; $F_{1,219} = 6.97$, $P = 0.0089$). However, both CFs (NR = 12.92 kHz, S.D. = 4.30; DE = 14.26 kHz, s.d. = 6.76; $F_{1,221} = 2.25$, $P = 0.14$) and Q40 were unchanged (NR = 2.39, s.d. = 1.23; DE = 2.16, s.d. = 1.21; $F_{1,113} = 0.94$, $P = 0.33$), although DE was associated with a significant increase in mean firing rate at the CF (DE mean @ CF = 2.26 spikes/s, s.d. = 2.37; NR mean @ CF = 0.93 spikes/s, s.d. = 1.14; $F_{1,221} = 24.18$, $P < 10^{-5}$). All statistical comparisons were carried out with ANOVA.

We examined population responses of neurons and used them to predict the identity of a stimulus by utilizing a classification method for temporal discharge patterns of neurons. These discharge patterns are first collected into sliding windows of various temporal resolutions (we used 1, 10 and 50 ms respectively). A greater resolution corresponds to greater length of the sliding window in the binless method used here, and ultimately refers to a coarser temporal

resolution of spikes. MDA (multiple discriminant analysis) estimates the probability with which each element of the stimulus matrix (21 frequencies X 7 levels) is assigned to the correct stimulus based on similarity between observed responses (spike count vectors derived by subtraction of spontaneous spike counts) to multiple repeats of the same stimulus (Campbell et al., 2010). This technique identifies a linear separation boundary between spike count vectors that are dissimilar to each other to classify unique spike patterns in response to a particular stimulus when multiple stimulus repeats are used. Given that each vector of spike counts from n≈175 sets of neuronal responses had that many degrees of freedom, we reduced the dimensionality to the first 20 principal components (PCs) of the *z*-scored spike count vectors that accounted for 60% of the variance in the samples. The MDA-based-classifier was trained to isolate clusters of responses with similar temporal discharge characteristics by forming a straight separation boundary between centroids of dissimilar clusters. Subsequently, we used a cross-validation model (Manel et al., 1999) that was fitted to a matrix of responses to predict the identity of a 'missing stimulus' that had been removed deliberately, yielding confusion matrices (e.g. **Fig. 6A**). Each confusion matrix contained the model-predicted identity of this missing stimulus as 'guessed' by the trained classifier. A perfect classifier assigns stimulus identities (*y*–axis) to the same location on the confusion matrix as that of the known stimulus value (*x*–axis) forming a diagonal of predicted stimulus identities. However, in reality a large number of classified responses are misclassified, and these are represented away from the diagonal. This classification was done for both frequency (ignoring level) and level (ignoring frequency) separately, for simplicity of comparisons. To identify the commonality of information between the known identity of the stimulus (*x*) and its predicted identity determined by the model above (*y*), we calculated mutual information (MI) between the two thus

$$MI\ (bits) = \sum_x \sum_y p(x,y) \log_2 \left(\frac{p(x,y)}{p(x)p(y)} \right)$$ **Equation 2**

We reduced the positive bias associated with MI via a bootstrapping approach, i.e. by resampling the datasets with randomly reassigned stimulus labels and subtracting the mean 'chance' MI for obtaining the bias-corrected MI (Panzeri et al., 2007). To determine whether the observed difference in the bias-corrected MI between the two groups of animals is significant or not, we used a permutation test wherein we pooled the data from the two groups. Once again, we calculated the bootstrapped difference in MI multiple times (n = 200, with each iteration additionally bootstrapped 40 times within each group) to arrive at the chance distribution of difference in MI. The observed difference in MI > 95% of values within a cumulative distribution of 'chance' difference implies one-tailed significance at $\alpha = 0.05$. For each of these comparisons, we calculated the unsigned error magnitude when assigning the predicted stimulus identity to the true identity of the stimulus. This error magnitude corresponds to the absolute deviation of the classified stimulus from the true, known stimulus identity. Similar to statistical assessment of MI differences, a bootstrapping approach was used to compare the observed difference in average absolute error magnitude to the hypothetical distribution of errors when the stimulus labels were randomly reassigned. Each of these comparisons was performed for the 3 different temporal resolutions and results are shown in main text.

Cortical Slice Preparation

Mice were anesthetized using isoflurane vapors. After the disappearance of the corneal reflex the brain was quickly dissected and immersed in ice-cold dissection buffer (in mM: 212.7 sucrose, 10 dextrose, 3 $MgCl_2$, 1 $CaCl_2$, 2.6 KCl, 1.23 $NaH_2PO_4 \cdot H_2O$, 26 $NaHCO_3$) which was bubbled with a 95% O_2/5% CO_2 gas mixture. Brain blocks containing primary visual and

auditory cortices were dissected and coronally sectioned into 300 μm thick slices using a Vibratome 3000 plus microslicer (Ted Pella, Redding, CA). Slices were then maintained in the dark at room temperature for 1 hour in a holding chamber containing artificial cerebrospinal fluid (ACSF, in mM: 124 NaCl, 5 KCl, 1.25 $NaH_2PO_4 \cdot H_2O$, 26 $NaHCO_3$, 10 dextrose, 2.5 $CaCl_2$ 1.5 $MgCl_2$, bubbled with 95% O_2/5% CO_2).

Light-evoked Sr^{2+}-mEPSCs

Slices were transferred to a submersion-type recording chamber mounted on the fixed stage of an upright microscope (E600 FN; Nikon, Tokyo, Japan) with oblique infrared (IR) illumination. AMPA receptor-mediated excitatory postsynaptic currents were isolated pharmacologically with 20 μM bicuculline and 100 μM DL-2-amino-5 phosphonopentanoic acid (DL-APV). These agents were added to modified ACSF containing 4 mM $MgCl_2$ and 4 mM $SrCl_2$ with 0 mM $CaCl_2$, which was bubbled with 95% O_2/5% CO_2, maintained at 30 ± 1 °C, and continually perfused at a rate of 2 ml/min. Slices were allowed to incubate in this solution for a minimum of 30 minutes prior to recording. Pyramidal neurons were identified visually in L4 and patched using a whole-cell patch pipette with a tip resistance between 3-5 MΩ, which was filled with internal solution containing in mM: 130 Cs-gluconate, 8 KCl, 1 EGTA, 10 HEPES, 4 ATP, 5 QX-314; pH 7.4, 285-295 mOsm). Biocytin (1 mg/ml) was added to the internal solution for post-hoc cell identification. ChR2 was activated using a 455-nm light emitting diode (LED) (ThorLabs DC2100) illuminated through a 40x objective lens, and controlled by a digital stimulator (Cygnus DG4000A). The minimal light intensity to elicit a reliable response was determined on a cell-by-cell basis with 5-ms duration remaining constant. Cells were held at -80 mV and recorded for a minimum of 10 minutes; event analysis was performed using mini

analysis software (see below). Data was acquired every 10 seconds for a duration of 1200 ms, which included a seal test pulse (100-ms duration), a 500-ms duration before LED illumination, and a 500-ms duration after LED illumination. A 400-ms window before LED was used for quantifying spontaneous desynchronized events (preLED), and a 400-ms window following a 50-ms delay from LED onset was used for quantifying LED-evoked desynchronized events (postLED). To calculate the amplitude of LEv-Sr^{2+}-mEPSCs corresponding to LED evoked desynchronized events without spontaneous desynchronized events, we used the following equation: [(postLED amplitude x postLED frequency) – (preLED amplitude x preLED frequency)]/ (postLED frequency – preLED frequency).

Recording of mEPSCs

AMPA receptor-mediated miniature excitatory postsynaptic currents were isolated pharmacologically with 1 μM tetrodotoxin (TTX), 20 μM bicuculline, and 100 μM DL-2-amino-5 phosphonopentanoic acid (DL-APV). These agents were added to ACSF bubbled with 95% O_2/5% CO_2 and maintained at 30 ± 1 °C, which was continually perfused at a rate of 2 ml/min. Cells in L4 were identified by their pyramidal-shaped soma and apical dendrite pointing towards the pia. Pyramidal neurons were patched using a whole-cell patch pipette with a tip resistance between 3-5 MΩ, which was filled with internal solution containing in mM: 130 Cs-gluconate, 8 KCl, 1 EGTA, 10 HEPES, 4 ATP, 5 QX-314; pH 7.4, 285-295 mOsm). Recordings were initiated 2-3 minutes after cell break-in. Biocytin (1 mg/ml) was included in the internal solution to confirm morphology and location of recorded cells. Axon patch-clamp amplifier 700B (Molecular Devices, Union City, CA) was used for voltage-clamp recordings. Cells were held at -80mV and the recorded mEPSC data was digitized at 10 kHz by a data acquisition board

(National Instruments, Austin, TX) and acquired through Igor Pro software (WaveMetrics, Lake Oswego, OR).

Acquired mEPSCs were analyzed with a Mini Analysis program (Synaptosoft, Decatur, GA), with a detection threshold set at 3 times the root mean square (RMS) noise level. Recordings were excluded from analysis if the RMS noise was >2, series resistance >25MΩ, and input resistance <100 MΩ. We also excluded all mEPSCs with a rise time >3 ms, and those showing a negative correlation between amplitude and rise time. 200 consecutive mEPSCs were analyzed from each cell, and the data is expressed as mean ± standard error of the mean. One factor analysis of variance (ANOVA) was used to analyze data across multiple groups, Student's t-test was used for two-group comparisons, and Kolmogorov-Smirnov test was used for cumulative probabilities. For all tests $P < 0.05$ was considered statistically significant.

Biocytin Processing

300 μm thick cortical slices were fixed in 4% paraformaldehyde overnight at 4°C. Slices were rinsed 2 x 10 minutes in 0.1 M phosphate buffer (PB) in mM: 19 $NaH_2PO_4 \cdot H_2O$, 81 Na_2HPO_4) at room temperature and permeabilized in 2% Triton X-100 in 0.1 mM PB for one hour. Slices were then incubated in avidin-AlexaFluor 633 conjugate diluted 1:2000 in 1% Triton X-100/0.1 M PB overnight at 4°C in the dark. After the incubation, slices were washed 2 x 10 minutes in 0.1 M PB and mounted on glass slides and allowed to dry overnight in the dark. Slides were cover-slipped with Prolong™ Anti-fade (Invitrogen) mounting media and sealed with nail polish. Images were taken using a Zeiss LSM 510 META confocal microscope.

Supplemental references

Campbell, R.A.A., Schulz, A.L., King, A.J., and Schnupp, J.W.H. (2010). Brief sounds evoke prolonged responses in anesthetized ferret auditory cortex. J. Neurophysiol. 103, 2783-2793.

Chase, S.M., and Young, E.D. (2007). First-spike latency information in single neurons increases when referenced to population onset. Proc. Natl. Acad. Sci. USA 104, 5175-5180.

Grimsley, J.M., Monaghan, J.J., and Wenstrup, J.J. (2011). Development of social vocalizations in mice. PLoS One 6, e17460.

Harris, K.D., Henze, D.A., Csicsvari, J., Hirase, H., and Buzsáki, G. (2000). Accuracy of tetrode spike separation as determined by simultaneous intracellular and extracellular measurements. J. Neurophysiol. 84, 401-414.

Hashimoto, Y., Iwasaki, S., Mizuta, K., Arai, M., and Mineta, H. (2007). Pattern of cochlear damage caused by short-term kanamycin application using the round window microcatheter method. Acta Otolaryngol. 127, 116-121.

Manel, S., Dias, J.M., and Ormerod, S.J. (1999). Comparing discriminant analysis, neural networks and logistic regression for predicting species distributions: a case study with a Himalayan river bird. Ecol. Model.120, 337-347.

Panzeri, S., Senatore, R., Montemurro, M.A., and Petersen, R.S. (2007). Correcting for the sampling bias problem in spike train information measures. J. Neurophysiol. 98, 1064-1072.

Victor, J.D. (2002). Binless strategies for estimation of information from neural data. Phys. Rev. E Stat. Nonlin. Soft Matter Phys. 66, 051903.

Walker, K.M.M., Bizley, J.K., King, A.J., and Schnupp, J.W.H. (2011). Multiplexed and robust representations of sound features in auditory cortex. J. Neurosci. 31, 14565-14576.